Journal of Power Sources 199 (2012) 110–116

Contents lists available at SciVerse ScienceDirect

Journal of Power Sources

journal homepage: www.elsevier.com/locate/jpowsour

Liquid phase migration effects on the evaporative and condensational dissipation of phosphoric acid in phosphoric acid fuel cell

Haruhiko Hirata[a,*], Tsutomu Aoki[b], Kazuyoshi Nakajima[c]

[a] Plant Engineering Department, Thermal & Hydro Power Systems & Services Div., Toshiba Corporation, 2-4, Suehiro-cho, Tsurumi-ku, Yokohama 230-0045, Japan
[b] Toshiba Fuel Cell Power System Corporation, Japan
[c] Metals Technology R&D Department, Power & Industrial Systems R&D Center, Toshiba Corporation, Japan

ARTICLE INFO

Article history:
Received 7 June 2011
Received in revised form 31 August 2011
Accepted 17 October 2011
Available online 20 October 2011

Keywords:
Phosphoric acid fuel cell
Evaporation
Condensation
Liquid phase migration
Numerical analysis

ABSTRACT

In phosphoric acid fuel cell (PAFC) stack, reduction of the phosphoric acid that is impregnated in the cell is a major factor to restrict the operating life. In this paper, the phosphoric acid reduction by the evaporative and condensational dissipation on the effect of liquid phase migration was evaluated by numerical analysis. The calculations that include the behavior of evaporation, condensation, and liquid phase migration for the phosphoric acid, and the behavior of gas flow and heat transfer were conducted for the model cell with conditions that correspond to an on site stack. The diffusion coefficient of liquid phase migration was derived from the activation energy and frequency factor based on the experimental results. The phosphoric acid distributions in the vapor phase and liquid phase at the process gas and electrode were calculated for the duration of 3136 h, and as a result of those, the exhausting and remaining amount of phosphoric acid for the cell were evaluated. The effects of liquid phase migration on the phosphoric acid dissipation were evaluated by analysis for various diffusion coefficients, and the analysis results were compared with the experimental results for the model cell.

1. Introduction

In phosphoric acid fuel cell (PAFC) stack, phosphoric acid that has low vapor pressure is used as an electrolyte to suppress the evaporation and dissipation with the process gases (the fuel and oxidant gases). However, the decrease in cell performance caused by the reduction of phosphoric acid is not negligible at the operating temperature of about 200 °C. For stacks that are designed to have an operating life of over 40,000 h, a basic design to keep low temperature at the gas exit comparing with the gas inlet of the cell is adopted. As a result of the design, the evaporated phosphoric acid in the process gas is condensed and recovered to the cell at the gas exit.

Yoshioka et al. have conducted experimental and numerical studies for evaporation [1] and condensation [2] of phosphoric acid. In those studies, the evaporation rate was treated to be controlled by the diffusion rate in the concentration boundary layer of process gas and the condensation rate was treated to be controlled by the cooling rate of process gas, and the phosphoric acid distributions in vapor and liquid phases and the recovery of phosphoric acid for the model cell were discussed.

In the previous paper [3], numerical analyses that include the behavior of evaporation and condensation for the phosphoric acid, and the behavior of gas flow and heat transfer were conducted for the model cell. Time series solutions for the phosphoric acid distributions in the vapor phase and liquid phase at the process gas and cell were calculated duration of 3300 h, and as a result of those, the exhausting and remaining phosphoric acids for the cell were evaluated.

In this paper, the liquid phase migration of phosphoric acid that has been eliminated in the previous paper was considered with the aim of investigation for more practical design method to estimate the precise dissipation of phosphoric acid. The diffusion coefficient of liquid phase migration was derived from the activation energy and frequency factor based on the experimental results for the substrate. Numerical analyses that include the behavior of evaporation, condensation, and liquid phase migration for the phosphoric acid, and the behavior of gas flow and heat transfer were conducted for the model cell that consists of porous electrode substrate and matrix with conditions that correspond to an on site stack. The phosphoric acid distributions in the vapor phase and liquid phase and the exhausting and remaining phosphoric acids for the model cell were calculated duration of 3136 h, and as a result of those, the exhausting and remaining phosphoric acids for the cell were calculated. The effects of liquid phase migration on the phosphoric acid dissipation were evaluated by calculations for the various diffusion

* Corresponding author. Tel.: +81 45 500 1539; fax: +81 45 500 1594.
E-mail address: haruhiko.hirata@toshiba.co.jp (H. Hirata).

0378-7753/$ – see front matter © 2011 Elsevier B.V. All rights reserved.
doi:10.1016/j.jpowsour.2011.10.063

Nomenclature

C_a	phosphoric acid volume (cm^3)
C_s	substrate pore volume (cm^3)
C	phosphoric acid specific volume
D	diffusion coefficient of liquid phase migration ($cm^2\ s^{-1}$)
C_0	initial phosphoric acid specific volume
t	time (s)
r	radial coordinate (cm)
I_0	modified Bessel function of 1st kind
a	phosphoric acid initial dispersion radius (cm)
$C\|_{r=0}$	central phosphoric acid specific volume
J	evaporated or condensed phosphoric acid flux ($mol\ s^{-1}\ cm^{-2}$)
$\Delta\tilde{G}^*$	activation energy change ($J\ mol^{-1}\ K^{-1}$)
$\tilde{c}$	frequency factor for J
c_F	frequency factor for diffusion coefficient
R	universal gas constant ($8.314\ J\ mol^{-1}\ K^{-1}$)
T	absolute temperature (K)

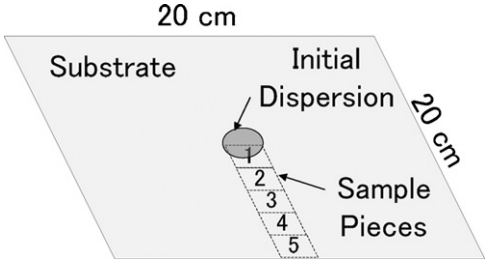

Fig. 1. Outline of liquid phase migration experiment.

coefficients, and the analysis results were evaluated by comparing with the experimental results.

2. Experimental methods and results

2.1. Liquid phase migration

The outline of the migration experiment is shown in Fig. 1, and the experimental conditions are shown in Table 1. The substrate size was 20 cm × 20 cm each, and the phosphoric acid that occupied 10% of the substrate pore volume (3.67 cc of 85 wt% H_3PO_4, 25 °C) was impregnated and dispersed uniformly by keeping in 50 °C air for 5 days. After that, the phosphoric acid (1.0 cc of 85 wt% H_3PO_4, 25 °C) was dropped at the center of substrate using an injection syringe and the initial dispersion radius was measured for each substrate. Each substrate was kept in various temperature conditions as shown in Table 1 for 1 day, and the phosphoric acid concentrations in each sample piece shown in Fig. 1 were measured using ICP-OES (Inductively Coupled Plasma Optical Emission Spectrometer, ICPS-5000/Shimadzu). The phosphoric acid concentrations were converted to the phosphoric acid volume (85 wt% H_3PO_4, 25 °C), and based on the phosphoric acid volume C_a and

Table 1
Conditions for liquid phase migration experiments.

Temperature	50, 100, 165, and 205 °C
Pressure	1 atm
Surrounding	Air + 60 °C humidified
Duration time	1 day
Fallen phosphoric acid	1 cc (85 wt% H_3PO_4, 25 °C)
Initial dispersion radius	2.1–2.8 cm

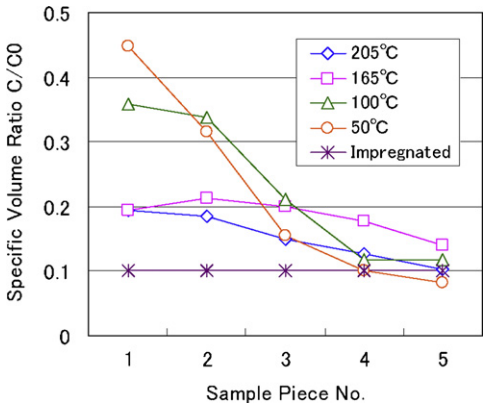

Fig. 2. Specific volume distributions after 1 day.

the substrate pore volume C_s, the phosphoric acid specific volume C was defined as follows.

$$C = \frac{C_a}{C_s} \tag{1}$$

Regarding to the time variable specific volume diffusion for the cylindrical symmetric one-dimensional direction that represents the radial coordinate of the substrate, the specific volume distribution was derived as follows.

$$C = \frac{C_0}{2Dt}\exp\left(\frac{-r^2}{4Dt}\right)\int_0^a \exp\left(\frac{-r'^2}{4Dt}\right) I_0\left(\frac{rr'}{2Dt}\right) r'dr' \tag{2}$$

Here, C_0 is initial specific volume of phosphoric acid at the substrate center and equals to 1.0 in each experiment, D is diffusion coefficient $cm^2\ s^{-1}$, t is time s, r is radial coordinate cm, r' is radial coordinate cm, I_0 is modified Bessel function of 1st kind, and a is initial dispersion radius cm of phosphoric acid.

The specific volume ratio distributions i.e. the specific volume distributions ($C/C_0 = C$) of the sample pieces for various temperatures are shown in Fig. 2. Based on these results, the central specific volumes $C|_{r=0}$ were derived by extrapolation for each case.

Regarding to the specific volume variation at the center of the cylindrical coordinate, the following equation was derived from Eq. (2) by substituting 0.0 for r.

$$C = C_0\left\{1 - \exp\left(\frac{-a^2}{4Dt}\right)\right\} \tag{3}$$

The diffusion coefficients D were derived by Eq. (3) according to $C|_{r=0}$, a, and t for each temperature condition. The derived diffusion coefficients are shown in Fig. 3, and the following equation was derived by regression of these results to the Arrhenius formula.

$$D = 6.89 \times 10^{-3} \times \exp\left(\frac{-1.50 \times 10^4}{RT}\right) \tag{4}$$

2.2. Evaporative and condensational dissipation

The outline of the model cell dissipation experiment is shown in Fig. 4, and the experimental conditions are shown in Table 2. The experiment was carried out using a porous electrode substrate and matrix in that the phosphoric acid was impregnated, and the steam humidified N_2 gas that substitute process gas was run through the electrode gas channel. The temperature in each electrode section was controlled by electrical heaters to correspond with the cell temperature distribution along the oxidant gas flow for an on site stack. The liquid phase phosphoric acid was able to migrate through the electrode sections, as there were no barriers between the electrode sections. The amount of the remaining phosphoric acid in

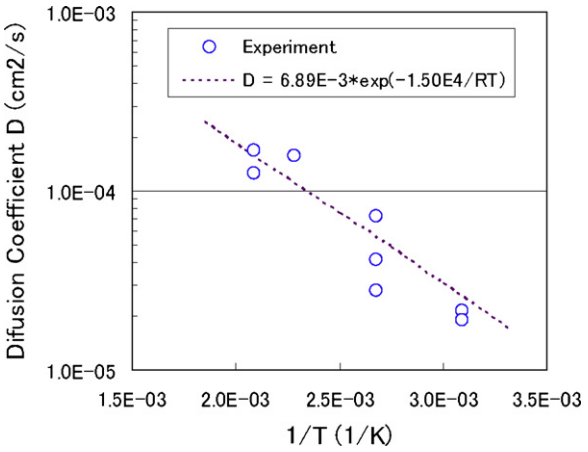

Fig. 3. Diffusion coefficient of liquid phase migration.

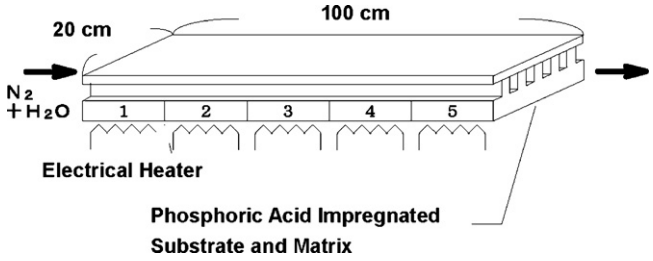

Fig. 4. Outline of model cell dissipation experiment.

Table 2
Conditions for dissipation experiment and analysis.

Pressure	1 atm
Gas flow rate	N_2 (8.3 l min^{-1}) + 60 °C humidified
Operation duration	3136 h
Initial phosphoric acid amount	9.6 cc (85 wt% H_3PO_4, 25 °C)/section

Temperature	Inlet	Section					Outlet
		1	2	3	4	5	
		205 °C	205 °C	201 °C	179 °C	163 °C	

each electrode section was derived from the quantitative analysis results by ICP-OES after 3136 h elapsed state,

3. Analysis method and conditions

For the calculations, the analysis code that was developed for a PAFC stack [3] was used with the addition of a function for the liquid phase migration. The previous code was based on the analysis code that has been developed for the characteristic calculation of a molten carbonate fuel cell (MCFC) stack [4], and the function of electrode reaction has modified to correspond to that of the PAFC and the functions for the evaporation and condensation of phosphoric acid have been added.

The phosphoric acid migrations in a PAFC stack are considered to be caused by the following two mechanisms.

(a) Migration accompanied with the phase change between liquid and vapor. That is dissipation of phosphoric acid from the porous electrode to process gas by evaporation and recovery from the process gas to porous electrode by condensation with the transfer by gas flow.

(b) Migration in the liquid phase. That is migration by capillary force caused by the concentration or temperature change of phosphoric acid in the porous electrode.

In the previous paper, the phenomenon above (a) was considered on the calculation. The phosphoric acid was regarded as a two components system of phosphorus pentoxide (P_4O_{10}) and water (H_2O), and the evaporation and condensation rates of phosphoric acid were derived by the following activation process based on the vapor liquid equilibrium of a two components system in reference [5–8] and the nucleation theory of a two components system in reference [9–12].

$$J = \tilde{c}\ \exp\left(\frac{-\Delta\tilde{G}^*}{RT}\right) \tag{5}$$

Here, J is the amount of evaporating or condensing phosphoric acid per unit area and unit time on the electrode surface mol s^{-1} cm^{-2}, R is the universal gas constant 8.314 J mol^{-1} K^{-1}, T is the liquid phase absolute temperature K, $\Delta\tilde{G}^*$ is the activation energy J mol^{-1}, and $\tilde{c}$ is the frequency factor.

In this paper, besides of the above phenomenon (a), the phenomenon (b) was considered, and the balance of phosphoric acid of liquid phase in the electrode was expressed as follows.

$$\frac{\partial C}{\partial t} = D\left(\frac{\partial^2 C}{\partial x^2} + \frac{\partial^2 C}{\partial y^2}\right) \tag{6}$$

Here, t is time, x and y are coordinates on the electrode surface, C is specific volume of the phosphoric acid, and D is diffusion coefficient derived by Eq. (4) as a function of T.

The unsteady analysis loop that includes the analysis loop of the code for MCFC was programmed. The behaviors of evaporation, condensation, liquid phase migration of the phosphoric acid were calculated, and as results of these, the amount of phosphoric acid in the vapor phase and liquid phase at the process gas and electrode were calculated in the unsteady loop.

Analyses were conducted on the conditions that correspond to the model cell experiment that was mentioned in Section 2.2, using a one dimensional model in the direction of the gas flow and each electrode section was divided into nine elements.

4. Analysis results

4.1. Amount of phosphoric acid in liquid phase at the electrode

The amount of remaining P_4O_{10} in each electrode section at 3136 h elapsed state for the analysis results and experimental result

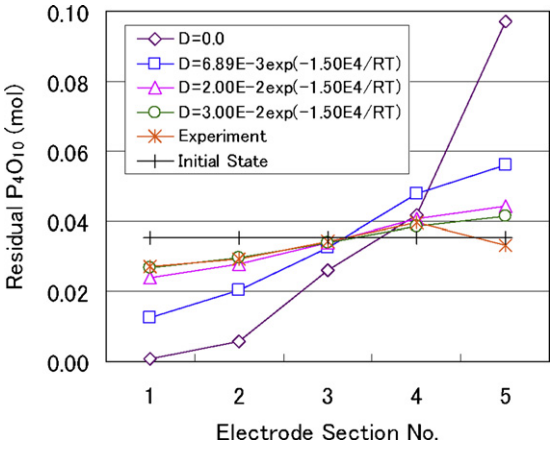

Fig. 5. Residual P_4O_{10} in the electrode.

are shown in Fig. 5. These were derived from the evaporation and condensation of P_4O_{10} and H_2O and the liquid phase migration of phosphoric acid that will be mentioned later. Here, besides of the diffusion coefficient shown in Eq. (4), the following diffusion coefficients were adopted for the analysis.

$$D = 0 \tag{7}$$

$$D = 2.00 \times 10^{-2} \times \exp\left(\frac{-1.50 \times 10^4}{RT}\right) \tag{8}$$

$$D = 3.00 \times 10^{-2} \times \exp\left(\frac{-1.50 \times 10^4}{RT}\right) \tag{9}$$

As shown in Fig. 5, there was little agreement between the analysis result derived from the diffusion coefficient of Eq. (4) and the experimental result, though the analysis result derived from the diffusion coefficient of Eq. (9) was in good agreement with the experimental result. Here, it should be noted that the electrode substrate and matrix were used for the dissipation experiments; on the other hand, the electrode substrate was used for the liquid phase migration experiments. As mentioned in [13], typical substrate is around 370 μm thickness and around 80% porosity, though typical matrix is around 50 μm thickness and lesser porosity. Therefore, in the electrode, the phosphoric acid is mainly reserved in the matrix that has lesser porosity comparing with the substrate and the liquid phase migration characteristic was considered to be mainly controlled by the matrix. In other words, the diffusion coefficient according to the electrode consists of substrate and matrix was considered to be different from the diffusion coefficient according to the substrate. Namely, it was considered that the diffusion coefficient of Eq. (4) showed that of the substrate, and the diffusion coefficient of Eq. (9) showed that of the electrode consists of substrate and matrix.

Consequently, the analysis result according to the diffusion coefficient of Eq. (9) was adopted for the comparison with the experimental result. The analysis results according to the diffusion coefficients of Eqs. (7) and (9) were discussed regarding the effect of the liquid phase migration that will have an influence on the phosphoric acid dissipation. Here, the analysis results according to the diffusion coefficient of Eq. (7) show the results eliminating the liquid phase migration.

In Fig. 5, after 3136 h, the amount of remaining P_4O_{10} for the analysis and experimental results increased according to the section goes to the gas outlet direction in each case. In sections 1 and 2, P_4O_{10} decreased from the impregnated P_4O_{10} at the initial state, and the dissipation of phosphoric acid to the process gas by evaporation was observed. In sections 4 and 5, there were more P_4O_{10} than the impregnated P_4O_{10}, and the recovery of phosphoric acid from the process gas by condensation was observed. The decreases of remaining P_4O_{10} in sections 1 and 2, and the increases in section 4 and 5 became lesser in accordance with the increase of liquid phase migration diffusion coefficient. These showed that the liquid phase migration deregulated the dissipation and recovery of P_4O_{10} by the evaporation and condensation. As a result of those, the residual P_4O_{10} decreased 0.00836 mol in section 1, and increased 0.00616 mol in section 5 for the diffusion coefficient of Eq. (9), though the residual P_4O_{10} decreased 0.0347 mol in section 1 and increased 0.0620 mol in section 5 for the diffusion coefficient of Eq. (7).

The total residual P_4O_{10} in the electrode for the various diffusion coefficient frequency factors c_F are shown in Fig. 6. The exhausted P_4O_{10} after 3136 h were 0.00475 mol and 0.00558 mol for the diffusion coefficient of Eqs. (7) and (9), respectively. As shown here, the difference of total exhausted P_4O_{10} for various liquid phase migration diffusion coefficients were a few. On the other hands, as mentioned about Fig. 5, the difference of decreasing P_4O_{10} in

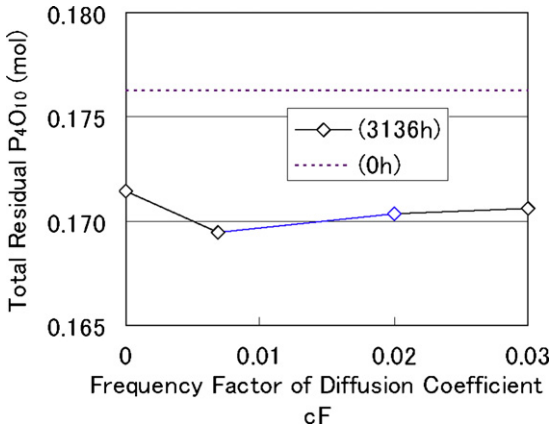

Fig. 6. Total residual P_4O_{10} in the electrode.

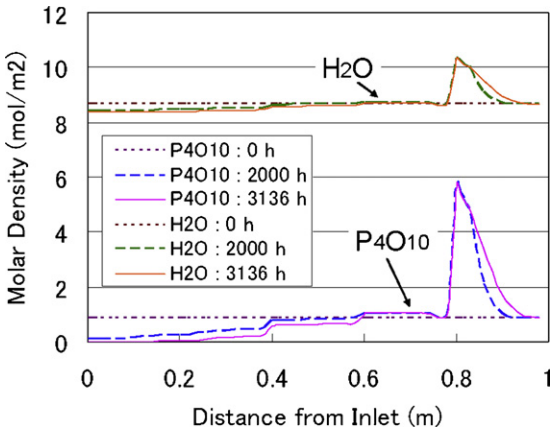

Fig. 7. P_4O_{10} and H_2O molar density of liquid phase. In the electrode, $D = 0.0$.

sections 1 and 2 for various liquid phase migration diffusion coefficients were much and the cell performance decline in these portion was considered to be fatal in the case of eliminated liquid phase migration. Consequently, the liquid phase migration had a big effect on the P_4O_{10} dissipation and on the cell performance through P_4O_{10} decrease in the sections of gas inlet side.

P_4O_{10} and H_2O molar concentration distributions in liquid phase at electrode along the gas flow direction at the initial, 2000 h, and 3136 h elapsed state for the diffusion coefficients of Eqs. (7) and (9) are shown in Figs. 7 and 8, respectively.

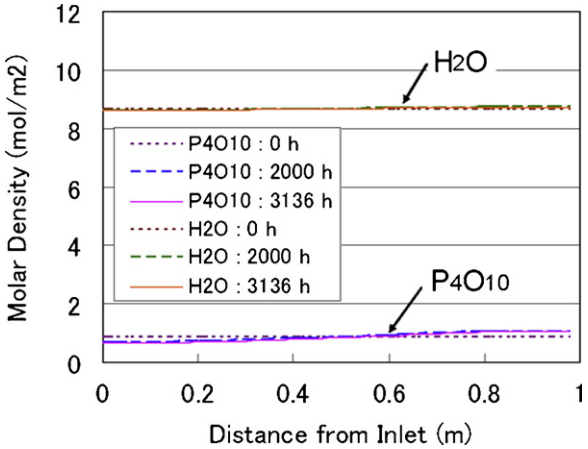

Fig. 8. P_4O_{10} and H_2O molar density of liquid phase. In the electrode, $D = 3.00E-2\exp(-1.50E4/RT)$.

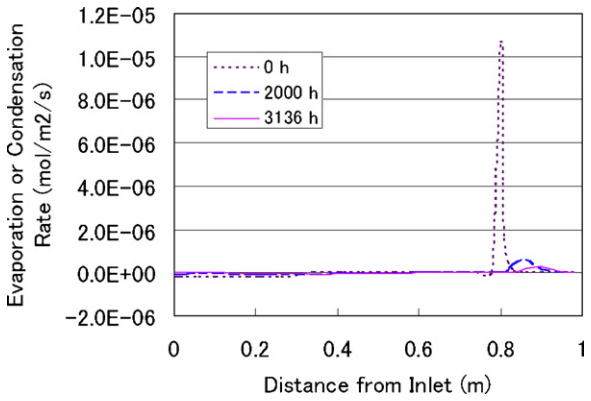

Fig. 9. Evaporation and condensation rates along the electrode, minus: evaporation, plus: condensation, $D = 0.0$.

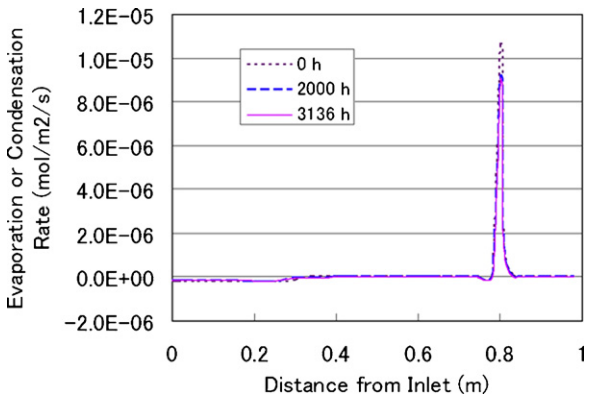

Fig. 10. Evaporation and condensation rates along the electrode, minus: evaporation, plus: condensation, $D = 3.00E-2\exp(-1.50E4/RT)$.

In the case for diffusion coefficient of Eq. (7), the molar concentration of P_4O_{10} and H_2O decreased at sections 1 and 2 these are 0.0–0.4 m distance from the gas inlet, and increased at section 5 that is 0.8–1.0 m distance from the gas inlet with the progress of time. Here, the decrease and increase of P_4O_{10} and H_2O molar concentration were caused by the evaporation and condensation accompanying gas flow transform, respectively. Since P_4O_{10} molar fraction of evaporating and condensing phosphoric acid were thicker than that of impregnated phosphoric acid (0.0922; 85 wt% H_3PO_4) in the electrode as it will be shown in Fig. 11, the variation of P_4O_{10} concentration in liquid phase at electrode was larger than the variation of H_2O concentration at sections 1, 2, and 5. It will be shown in Fig. 9, the peak position of evaporation and condensation rates moved toward the gas downstream and these rates decreased with the time progress. These were correspondent with the decrease and increase of the molar concentration of P_4O_{10} and H_2O in the liquid phase according to the gas flow for the evaporation and condensation, respectively, in Fig. 7.

In the case for diffusion coefficient of Eq. (9), the molar concentration of P_4O_{10} and H_2O decreased at sections 1 and 2, and increases at section 5 with the progress of time. In this case, the change for molar concentration of P_4O_{10} and H_2O in each section was lesser than the case for the diffusion coefficient of Eq. (7). These were caused by the liquid phase phosphoric acid recirculation from section 5 to sections 1 and 2 by liquid phase migration, and as result of that, the liquid phase conditions were kept almost stable through the 3136 h duration. On the other hands, the liquid phase phosphoric acid conditions were continuously changed with the progress of time, as the liquid phase migration was eliminated in the case of Fig. 7.

4.2. Evaporation and condensation rates of phosphoric acid

The evaporation and condensation rate distributions of phosphoric acid along the gas flow direction for the initial, 2000 h, and 3136 h elapsed state for the diffusion coefficient of Eqs. (7) and (9) are shown in Figs. 9 and 10, respectively. Here, the negative rate shows evaporation and positive rate shows condensation in each figure.

In the case for diffusion coefficient of Eq. (7), the evaporation arose at sections 1 and 2, and the condensation arose at section 5 where the electrode temperature steeply fell comparing with the upstream. The peak magnitude of evaporation and condensation rate fell in accordance with the progress of time, and the peak position of evaporation and condensation rate gradually moved to the downstream of gas flow.

In the case for diffusion coefficient of Eq. (9), at the initial state, the evaporation and condensation rate distribution was the same

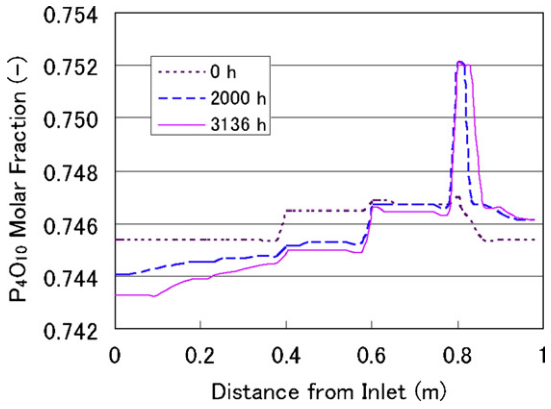

Fig. 11. P_4O_{10} molar fractions of evaporating and condensing phosphoric acid along the electrode, $D = 0.0$.

as the case for the diffusion coefficient of Eq. (7). However, the peak magnitude and position of evaporation and condensation rate were almost stable in the progress of time. These showed that the liquid phase phosphoric acid migrated from section 5 to sections 1 and 2 in the progress of time, and were correspondent with the difference between the results of Figs. 7 and 8.

P_4O_{10} molar fraction distribution of evaporating and condensing phosphoric acid composition along the gas flow direction for the diffusion coefficients of Eqs. (7) and (9) are shown in Figs. 11 and 12, respectively.

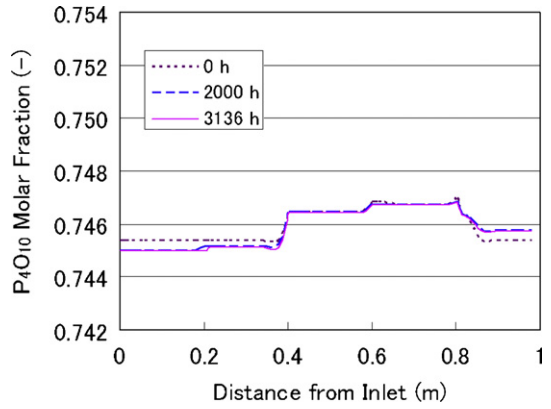

Fig. 12. P_4O_{10} molar fractions of evaporating and condensing phosphoric acid along the electrode, $D = 3.00E-2\exp(-1.50E4/RT)$.

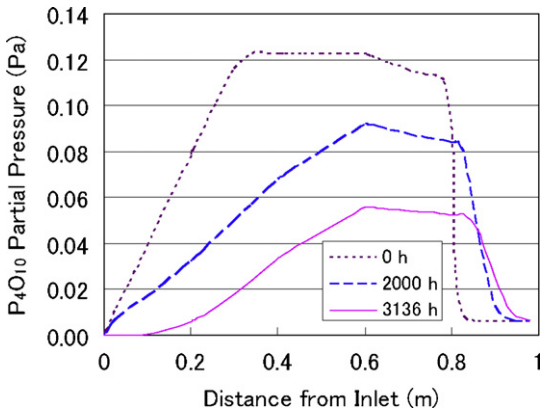

Fig. 13. P_4O_{10} partial pressure along the electrode, $D = 0.0$.

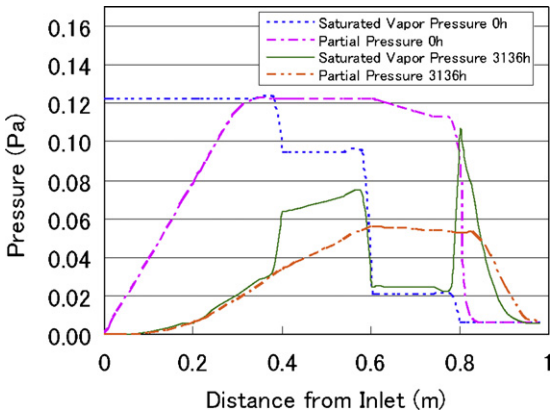

Fig. 15. P_4O_{10} saturated vapor pressure and partial pressure along the electrode, $D = 0.0$.

In the cases for diffusion coefficient of Eq. (7), P_4O_{10} molar fraction of evaporating composition at sections 1, 2, and 3 fell in accordance with the time progress, and P_4O_{10} molar fraction changed from 0.745 to 0.743 in section 1 through the 3136 h duration. In condensing composition at section 5, P_4O_{10} molar fraction increased in according with the time progress, and changed from 0.747 to 0.752 through the 3136 h duration.

In the cases for diffusion coefficient of Eq. (9), P_4O_{10} molar fraction change of evaporating and condensing compositions in the time progress were lesser than the cases for diffusion coefficient of Eq. (7), and P_4O_{10} molar fraction change was from 0.7454 to 0.7450 at section 1 and from 0.7454 to 0.7457 at section 5 through the 3136 h duration.

P_4O_{10} concentration of evaporating and condensing compositions were thicker than the molar fraction 0.0922 (85 wt% H_3PO_4, 25 °C) of impregnated phosphoric acid for each case.

4.3. Partial pressure and saturated vapor pressure of phosphoric acid

P_4O_{10} partial pressure distributions of vapor phase in the process gas along the gas flow direction at the initial, 2000 h and 3136 h elapsed states for the diffusion coefficients of Eqs. (7) and (9) are shown in Figs. 13 and 14, respectively.

In the case for diffusion coefficient of Eq. (7), at the initial state, P_4O_{10} partial pressure increased gradually along the gas flow in sections 1 and 2 where evaporation occurred, and decreased steeply and reached to fixed values in section 5 where condensation occurred. The gradual increases at section 1 and steep decrease at section 5 for P_4O_{10} partial pressures were correspondent with the gradual decrease of the evaporation rate at section 1 and the steep increase of condensation rate at section 5 in Fig. 9. The increase of P_4O_{10} partial pressures at the gas inlet part became lesser according to the progress of time, and the distance between the gas inlet and the position where the vapor pressure reached to saturation became long. P_4O_{10} partial pressure at the gas exit that determines the amount of exhausting phosphoric acid slightly increased from 0.00603 Pa to 0.00654 Pa in the duration of 3136 h.

In the case for diffusion coefficient of Eq. (9), at the initial state, P_4O_{10} partial pressure distribution was the same as the case for the diffusion coefficient of Eq. (7). The changes of P_4O_{10} partial pressures distributions according to the progress of time were lesser than the case for diffusion coefficient of Eq. (7) and P_4O_{10} partial pressure distributions were almost stable except sections 3 and 4 in the duration of 3136 h. These showed the effect of the phosphoric acid liquid phase migration from section 5 to sections 1 and 2, and were correspondent with the steadiness for the evaporation and condensation rates with the progress of time as shown in Fig. 10. P_4O_{10} partial pressure was around 0.00603 Pa on the gas exit at 3136 h elapsed state, and it was almost same as that of the case for diffusion coefficient of Eq. (7). This caused the total residual P_4O_{10} to be almost same between the cases for diffusion coefficients of Eqs. (7) and (9) as shown in Fig. 6.

P_4O_{10} partial pressure in the vapor phase and P_4O_{10} saturated vapor pressure that was determined by the condition in liquid phase at electrode at initial state and 3136 h elapsed state for the diffusion coefficients of Eqs. (7) and (9) are shown in Figs. 15 and 16, respectively.

In the case for diffusion coefficient of Eq. (7), at the initial state, P_4O_{10} partial pressure at the gas inlet part was lower than the

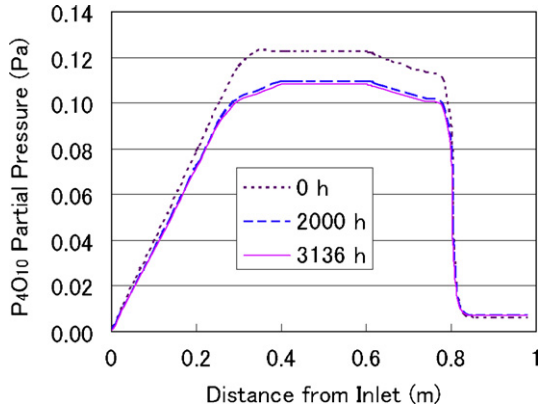

Fig. 14. P_4O_{10} partial pressure along the electrode, $D = 3.00E-2\exp(-1.50E4/RT)$.

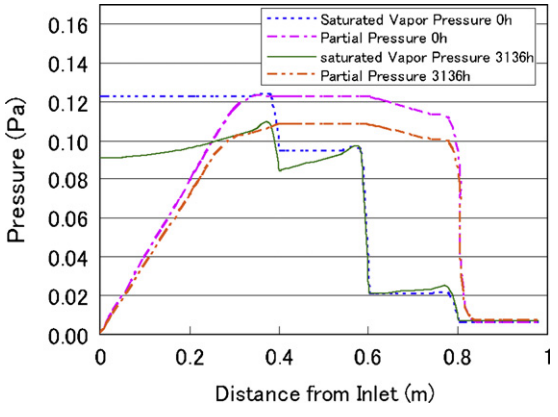

Fig. 16. P_4O_{10} saturated vapor pressure and partial pressure along the electrode, $D = 3.00E-2\exp(-1.50E4/RT)$.

saturated vapor pressure, and according to the gas flow the partial pressure increased and reached to saturation. At sections 3 and 4 these are 0.4–0.8 m distance from the gas inlet, P_4O_{10} partial pressure was higher than the saturated vapor pressure and the vapor phase of process gas was supersaturating state regarding to the temperature and phosphoric acid concentration in the liquid phase at the electrode. At section 5, P_4O_{10} partial pressure decreased steeply and reached to saturated vapor pressure according to the liquid phase conditions at the gas exit.

At the 3136 h elapsed state, P_4O_{10} saturated vapor pressure increased from 0 according to the gas flow, and P_4O_{10} partial pressure distribution was almost equal to the saturated vapor pressure distribution in sections 1 and 2. P_4O_{10} saturated vapor pressure decreased comparing with the initial state, as the liquid phase phosphoric acid concentration was decreased because of the thicker evaporating P_4O_{10} concentration as shown in Fig. 11. P_4O_{10} partial pressure was supersaturating state at section 4, and decreased gradually at section 5 to reach to the saturated vapor pressure at the gas exit. The saturated vapor pressure steeply rose at the gas inlet portion of section 5 because of the steep increase of P_4O_{10} concentration in the electrode by condensation as shown in Fig. 7.

In the case for diffusion coefficient of Eq. (9), at the initial state, P_4O_{10} partial pressure and saturated vapor pressure distributions were the same as the case for the diffusion coefficient of Eq. (7) in each.

At the 3136 h elapsed state, P_4O_{10} saturated vapor pressure increased from 0 according to the gas flow, and P_4O_{10} partial pressure distribution was lower than the saturated vapor pressure distribution in sections 1 and 2. P_4O_{10} saturated vapor pressure was lower comparing to the initial state, however the difference was lesser than the case for diffusion coefficient of Eq. (7). The difference of P_4O_{10} partial pressure distributions between the initial state and 3136 h elapsed state was also lesser than the case for diffusion coefficient of Eq. (7). P_4O_{10} partial pressure was supersaturating state at sections 3 and 4, and it decreased steeply at section 5 to reach to the saturated vapor pressure at the gas exit. The saturated vapor pressure at section 5 was almost same through the duration of 3136 h; this was caused by the steadiness of phosphoric acid in section 5 by the liquid phase migration from section 5 to sections 1 and 2. This was correspondent with the steadiness in the progress of time for the evaporation and condensation rates and liquid phase molar densities of phosphoric acid as shown in Figs. 10 and 8, respectively.

5. Conclusion

The dissipation characteristics of phosphoric acid in PAFC were evaluated by the analysis using a code that includes the behavior of the evaporation, condensation, and liquid phase migration of phosphoric acid and gas flow and heat transfer. The analysis was conducted for the model cell consists of porous electrode substrate and matrix that has correspondent conditions for an on site stack in the duration of 3136 h.

The liquid phase migration of phosphoric acid were calculated using an Arrhenius formula diffusion coefficients derived from experimental result for substrate, and the phosphoric acid dissipation characteristic for each electrode section was calculated. The analysis results had good agreement with the experimental results by adopting appropriate frequency factor for diffusion coefficient. Consequently the effectiveness of the present analysis method was validated.

The effects of liquid phase migration on the phosphoric acid dissipation were evaluated by comparing the analysis results including the liquid phase migration and eliminating that. In the case of eliminating liquid phase migration, the amount of remaining P_4O_{10} decreased in the high temperature sections at gas inlet side and increased in the low temperature sections at gas outlet side through the 3136 h duration. Namely, P_4O_{10} in the gas inlet sections migrated to the gas outlet sections by the evaporation and condensation accompanied with gas flow. On the other hand, in the case of including liquid phase migration, P_4O_{10} decrease and increase in the high and low temperature sections were lesser than the above case. As a result of that, P_4O_{10} migrations from the gas inlet sections to the gas outlet sections were lesser than the case of eliminating liquid phase migration. Consequently, it was observed that the liquid phase migration deregulated the effect of migration by the evaporation and condensation accompanied with gas flow.

Both cases of including and eliminating liquid phase migration, P_4O_{10} partial pressure was affected by the conditions of the vapor phase in process gas and the liquid phase in electrode, and for some conditions, P_4O_{10} partial pressure could be higher than the saturated vapor pressure according to the liquid phase in the electrode, and the supersaturating states were resulted to be possible.

As a result of these, the remaining distribution and exhausting amount of P_4O_{10} for the electrode were estimated in detail.

References

[1] S. Yoshioka, K. Mitsuda, H. Horiuchi, M. Matsumoto, Denki Kagaku 65 (4) (1997) 314–319.
[2] S. Yoshioka, K. Mitsuda, H. Horiuchi, M. Matsumoto, Denki Kagaku 66 (1) (1998) 41–47.
[3] H. Hirata, T. Aoki, K. Nakajima, Journal of Power Sources 196 (2011) 8004–8011.
[4] H. Hirata, M. Hori, Journal of Power Sources 63 (1996) 115–120.
[5] J.H. Dean, Lange's Handbook of Chemistry, 1973, pp. 10–28.
[6] E.H. Brown, C.D. Whitt, Industrial and Engineering Chemistry 44 (3) (1952) 615–618.
[7] J.M. Prausnitz, Molecular Thermodynamics of Fluid Phase Equilibria, 1985, p. 192.
[8] Chemical Society of Japan, The Chemistry Manual Basic, vol. II, 1993, pp. II–117.
[9] H. Reiss, Journal of Chemical Physics 18 (6) (1950) 840–848.
[10] W. Studzinski, G.H. Spiegel, R.A. Zahoransky, Journal of Chemical Physics 84 (7) (1986) 4008–4014.
[11] M. Kulmala, A. Laaksonen, Journal of Chemical Physics 93 (1) (1990) 696–701.
[12] T. Keii, Reaction Kinetics, 1983, p. 88.
[13] W. Vielstich, H.A. Gasteiger, A. Lamm, Handbook of Fuel Cells, vol. 4, 2003, pp. 811–831.